Molecular Crystals and Liquid Crystals

ISSN: 1542-1406 (Print) 1563-5287 (Online) Journal homepage: http://www.tandfonline.com/loi/gmcl20

Investigation of a Naphthalimide Based OH^- Sensor with Quinoline Attached

Xiaochuan Li, Yuhe Zhou, Yingchao Zhang & Young-A Son

To cite this article: Xiaochuan Li, Yuhe Zhou, Yingchao Zhang & Young-A Son (2015) Investigation of a Naphthalimide Based OH^- Sensor with Quinoline Attached, Molecular Crystals and Liquid Crystals, 622:1, 84-93, DOI: 10.1080/15421406.2015.1097004

To link to this article: http://dx.doi.org/10.1080/15421406.2015.1097004

Published online: 16 Dec 2015.

Mol. Cryst. Liq. Cryst., Vol. 622: pp. 84–93, 2015

ISSN: 1542-1406 print/1563-5287 online
DOI: 10.1080/15421406.2015.1097004

Investigation of a Naphthalimide Based OH^- Sensor with Quinoline Attached

XIAOCHUAN LI,[1,2,*] YUHE ZHOU,[1] YINGCHAO ZHANG,[1] AND YOUNG-A SON[3,*]

[1]Collaborative Innovation Center of Henan Province for Green Manufacturing of Fine Chemicals, Key Laboratory of Green Chemical Media and Reactions, Ministry of Education, Henan Normal University, Xinxiang, Henan, P. R. China
[2]Henan Key Laboratory of Green Chemical Media and Reactions, School of Chemistry and Chemical Engineering, Henan Normal University, Xinxiang, Henan, P. R. China
[3]BK21, Department of Advanced Organic Materials Engineering, Chungnam National University, Daejeon, South Korea

In this contribution, a sensitive colorimetric chemosensor was constructed based on the framework of naphthalimide. And it was characterized by NMR and mass spectroscopic techniques. The solution color changed from yellowish to deep blue with the addition of OH^-. The obvious color change can be distinguished by naked eye. Excellent selectivity against other common anions was also observed. Even if the strong Lewis base F^- added to the dye solution, no color change was induced. The effects imposed on the obvious color change can be ascribed to the deprotonation of –NH– of bridge unit. The results of structural optimization and molecular orbital calculation uncovered the underlying signal mechanism. Due to the depronotion effect, lowered energy gap (HOMO/LUMO) and electron redistribution leads to the red-shift of longest maximum absorption.

Keywords colorimetric chemosensor; naphthalimide; selectivity; deprotonation effect; signal mechanism.

Introduction

Small fluorescent molecules have been developed rapidly due to the easy structural modification and tunable photophysical properties toward the targeted functions [1–6]. The development of highly efficient fluorophores is essential in application of sensors [7–10], optical switches [11, 12], molecular motors [13, 14], logic gates [15], and organic-light-emitting diodes (OLEDs) [16]. Among various of fluorophores, 1,8-naphthalimide is one

*Address correspondence to Young-A Son, Department of Advanced Organic Materials Engineering, Chungnam National University, 220 Gung-dong, Daejeon 305-764, South Korea, Email: yason@cnu.ac.kr and Xiaochuan Li, Collaborative Innovation Center of Henan Province for Green Manufacturing of Fine Chemicals, Key Laboratory of Green Chemical Media and Reactions, Ministry of Education,Henan Normal University, Xinxiang, Henan, P. R. China. E-mail: lixiaochuan@htu.cn.

Color versions of one or more of the figures in the article can be found online at www.tandfonline.com/gmcl.

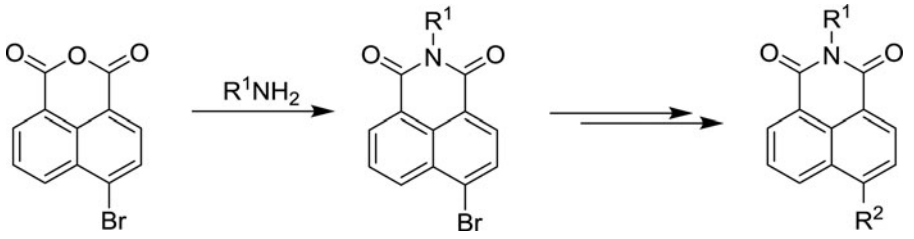

Scheme 1. General procedure for the modification of 1,8-naphthalimide framework.

of the typical chromophores. Due to the conveniently synthesis of naphthalimide framework, it has been widely used in designing various functional molecules. Additionally, the commercially available 1,8-naphthalic anhydride allows the mass production of its derivatives. The naphthalimide ring can be conveniently substituted at the 4-position by amino or nitro groups, which facilitates the introduction of other functional groups and induces major effect on the electronic properties with a consequent influence on the chemical, photochemical and spectroscopic properties. Now, 1,8-naphthalimide brominated at the 4-position of the ring has been proposed as good candidates for the production of photoelectric material (Scheme 1). It has been demonstrated as a well-received molecule by its application as fluorescent brighteners [17], fluorescent bioprobes [18, 19], as solar energy collectors [20] and laser dyes [21]. The rich optical properties of 1,8-naphthalimides, together with their easy synthesis in high purity on a large scale, opens up broad applications within the material and bio-technology field.

In this article, a newly designed 1,8-naphthalimide derivative, conceived as suitable candidates for OH^- sensor. It is known to all that the key point of the rich optical properties of 1,8-naphthalimides is depends on the nature of the substituents, in particular at the 4-position. Electron-donating or electron-withdrawing groups at the 4-position determine the existence of a strongly fluorescent lowest lying charge-transfer excited state and marked reducing or oxidizing capability. Here, quinolone was condensed with 1,8-naphthalimide and connected by the bridge unit –NHN-. Any disturbance occurred at the bridge unit will lead to change of optical properties, which will be discussed.

Experimental

General Procedures and Materials

The solvents used in the reaction were carefully dried according to the standard procedure and stored over 4Å molecular sieve. All the reagent-grade chemicals were purchased from Sigma-Aldrich CO. LLC. (South Korea) and used without further purification. All synthesized compounds were routinely characterized by TLC and ^{1}H NMR. TLC was performed on aluminum-backed silica gel plates (Merck DC. Alufolien Kieselgel 60 F254).

^{1}H and ^{13}C NMR Spectroscopy

^{1}H and ^{13}C nuclear magnetic resonance (NMR) spectra were recorded on a Brucker AM-400 spectrometer operating at frequencies of 400 MHz for proton 100 MHz for carbon in DMSO-d_6. Proton chemical shifts (δ) are relative to tetramethylsilane (TMS, $\delta = 0$) as internal standard and expressed in parts per million. Spin multiplicities are given as *s*

(singlet), *d* (doublet), *t* (triplet), and *m* (multiplet) as well as *b* (broad). Coupling constants (*J*) are given in Hertz.

Mass and High Resolution Mass Spectra (HRMS)

The mass spectra measured on a LC-MS (Waters UPLC-TQD) mass spectrometer. High resolution mass spectra (HRMS) were measured on a Brucker microOTOF II Focus instrument.

UV-Vis and Emission Spectra

The absorption spectra were measured with a PERSEE TU-1900 and an Agilent 8453 spectrophotometer. Emission spectra were measured with Shimadzu RF-5301PC fluorescence spectrophotometer. The solvents used in photochemical measurement were spectroscopic grade and were purified by distillation. The stock solution of compounds (2×10^{-3} M) was prepared in THF, and a fixed amount of these concentrated solutions were added to each experimental solution. [OH^-] was prepared by NaOH dissolved in distilled water (5×10^{-2} M). All the experiments were done repeatedly, and reproducible results were obtained. Prior to the spectroscopic measurements, solutions were deoxygenated by bubbling nitrogen through them.

Theoretical Calculations

For the theoretical study of excited state photo-physics of the compound, the *DMol*[3] program packaged in *Material Studio* (Accelrys Software Inc., United States) was used [22, 23]. The ground state geometries and the frontier molecular orbital of the compound were calculated using the density function theory (DFT) with the B3LYP hybrid functional and the double numerical plus *d*-functions (DNP) atomic orbital basis set.

Synthesis

The synthetic route of the target compound, 2-butyl-6-(2-(quinoline-2-yomethylene)hydrazinyl)-benzo- isoquinoline-1,3-dione (**NQ**), was outlined in Scheme 2. 4-Bromo-1,8-naphthalic anhydride (**1**) is commercial available and used without further purification. **2** was obtained by refluxing an equivalent amount of butyl amine in ethanol, which has been well documented [24, 25]. The bromine atom, located at 4-position of 1,8-naphthalimide, can be easily substituted by hydrazine hydrate and gave **3**. Subsequent condensation between **3** and quinoline-2-carbaldehyde yielded the target **NQ**.

2-Butyl-6-hydrazinyl-1,8-naphthalimide (**3**) (71 mg, 0.25 mmol) and quinoline-2-carbaldehyde (39 mg, 0.25 mmol) dissolved in methanol (10 mL). The mixture was stirred at room temperature for 24 h. During the reaction, a large amount of yellow solid was precipitated out from methanol. The precipitant was collected and washed carefully with cold methanol. Pure sample was obtained by recrystallization from ethanol and yielded 94 mg product (89%).

^{1}H NMR (400 MHz, DMSO-d_6) δ 11.76 (s, 1H), 8.79 (d, J = 8.0 Hz, 1H), 8.56 (s, 1H), 8.48 (d, J = 8.0 Hz, 1H), 8.39 (d, J = 8.0 Hz, 2H), 8.24 (d, J = 8.0 Hz, 1H), 8.00 (m, 2H), 7.87 – 7.78 (m, 3H), 7.63 (d, J = 8.0 Hz, 1H), 4.01 (s, 2H), 1.62 – 1.58 (m, 2H), 1.36-1.32 (m, 2H), 0.93 (t, J = 8.0 Hz, 3H); ^{13}CNMR (100 MHz, DMSO-d_6): δ 163.2, 156.4,155.1, 145.3, 136.5, 135.8, 133.3, 132.4, 131.9, 131.5, 131.1, 130.5, 130.1,

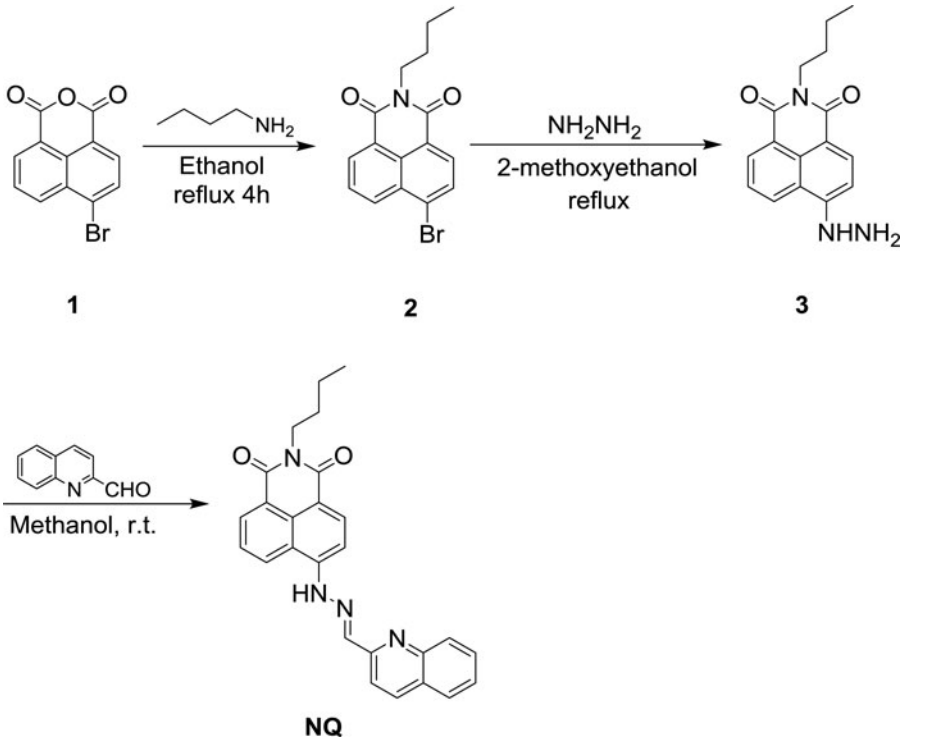

Scheme 2. Synthesis of 2-butyl-6-(2-(quinoline-2-yomethylene)hydrazinyl)-benzoisoquinoline-1,3-dione (**NQ**).

129.2, 128.0, 122.6, 122.1, 42.5, 30.7, 20.5, 14.1. EI^+/MS m/z 422$[M]^+$. HRMS calcd for $C_{26}H_{22}N_4O_2$ 422.1743, found 422.1744.

Result and Discussion

The absorption spectra of **NQ** was measured in DMF with the concentration 2.0×10^{-5} M at room temperature and shown in Figure 1. An intense absorption peak was observed at 472 nm ($\varepsilon = 2.4 \times 10^4\ M^{-1}cm^{-1}$). Generally, it was induced by the intramolecular charge transfer N substituted at the 4-position of naphthalimide framework. Obviously, the proton attached to the bridging N atom can be deprived by base. The effects of deprotonation and protonation of a 2.0×10^{-5} M of **NQ** in DMF, occurred to the bridge N atom, were investigated in detail. The titration spectra of OH^- were shown in Figure 1. Upon the addition of OH^-, the longest absorption maximum at 472 nm decreased gradually and a new absorption band, centered at 610 nm, appeared. The isosbestic point ($\lambda = 508$ nm), observed in Figure 1, suggests that the only two species co-exist in the solution, which in this case are the deprotonation and protonation species of **NQ**. With the OH^- addition reached to 8 equivalent of **NQ**, the absorption intensity at 610nm reached to the maximal value ($A = 0.14$, $\varepsilon = 7.1 \times 10^3\ M^{-1}cm^{-1}$). At the same time, the yellowish solution turned to bluish gradually. A satisfactory linear relationship between absorption intensity and the molar equivalent of OH^- was found with the correlation coefficient as high as 0.9961 with the OH^- varied from 0 to 8 equivalent, indicating effective interaction between OH^- and

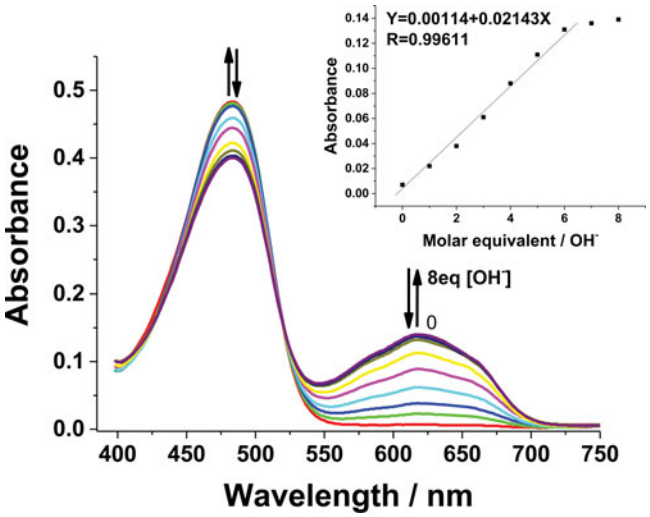

Figure 1. Absorption change of **NQ** in DMF (2.0×10^{-5} M) imparted by deprotonation/protonation. 10 μL [OH^-] (5.0×10^{-2} M) was added each time to **NQ** (2.5 mL DMF solution in quartz cell) until equilibrium between NQ and OH^- was established. Insert: dependence of absorption in intensity at 618 nm with respect to molar equivalent of OH^- ion.

–N*H*–. Upon addition of H^+, the blue solution color faded and the yellowish solution color recovered. A reversible yellow/blue color transformation can be established by alternated addition of OH^-/ H^+. Unlike some of the published naphthalimides, typical green emission was not observed with or without the addition of base. The quantum yield of **NQ** in DMF was estimated to be lower than 1%. And no fluorescence enhancement was found by the addition of OH^-/H^+. The base/acid induced color change, corresponding to the absorption behavior, can be ascribed to the deprotonation of the **NQ** dye. It also demonstrated that

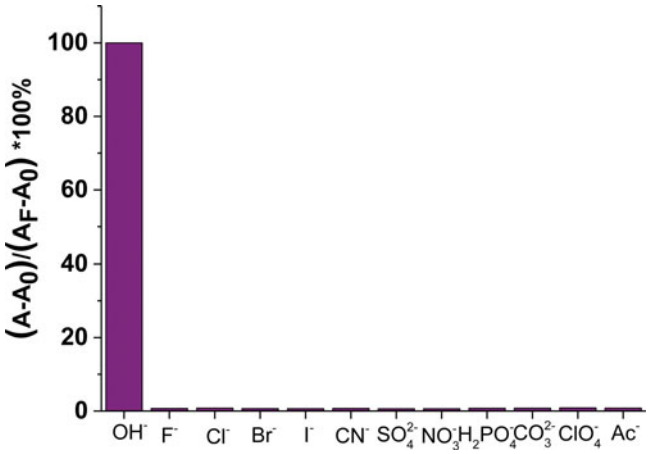

Figure 2. Comparison of percent increase of absorption of **NQ** in DMF solution at 610 nm in the presence of 10 equivalents of various anions.

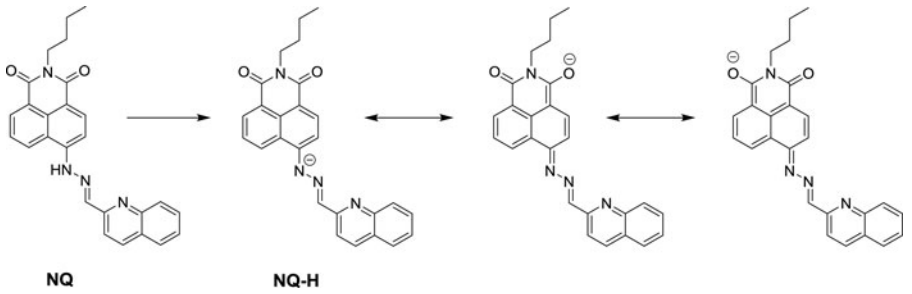

Scheme 3. Concept of deprotonation.

the electronic effect of 4-position substituents was essential to the physical properties of naphthalimiides [26].

The interactions of deprotonaion from nitrogen atom by others anions were also investigated. Apart from OH^-, no observable absorption change was found by addition of other anions, such as Cl^-, Br^-, I^-, SO_4^{2-}, NO_3^-, $H_3PO_4^-$, CO_3^{2-}, ClO_4^-, and CO_3^{2-}. Even if the strong Lewis F^- was incubated, the proton of nitrogen atom cannot be captured. Figure 2 shows the binding property toward different anions. The absorption enhancement at 610 nm induced by the same amount (10μM) of OH^- was estimated to be 140-fold (F^-). Due to the similar size between fluorine and hydrogen, the molecular topology was altered significantly, and hence little interaction would be expected in the corresponding absorption spectra. The proposed sensing mechanism was outlined in Scheme 3. Once the proton of –NH– was deprived, the electron density of N atom will be increased significantly, which will lead to efficient charge transfer process and red-shift the longest absorption maximum. It should be noted that the proton of hydrazone is difficult to be captured than that of acylhydrazine [10, 27, 28].

To better comprehend the geometrical, electronic, and optical properties of **NQ**, we undertook a comprehensive computational investigation on the platform of Material Studio. To reduce the run times in the first instance, the ground-state energy-minimized structures were calculated using DFT and LDA/DN basis set [22, 23]. Further refinement and optimization on structures were then undertaken using DFT/B3LYP/DNP basis set. The calculated electrostatic potentials for the **NQ** and **NQ-H** were shown in Figure 3. Not surprisingly, once the proton was captured, the electron rich N atom polarizes the electrostatic potential at this site.

The size and signs of the frontier molecules orbitals were illustrated in Figure 4.

The optics calculation of **NQ** indicated that the HOMO→LUMO transition contributes significantly to the longest absorption maximum of **NQ** with the oscillator strength (f) 0.726. The energy level between HOMO and LUMO was calculated to be 2.50eV (corresponding to the 497 nm absorption), which is close to the experimental value 472 nm. The transition of HOMO-1→LUMO and HOMO→LUMO+1 also contributed to the absorption of **NQ**, but the oscillator strength of the two transitions was very weak with the f being 0.010 and 0.056. Once the proton was deprived from –NH–, the electron transitions were also altered and the electron transitions were more complicated than that of **NQ**. In **NQ-H**, the transition of HOMO–1→LUMO, HOMO→LUMO+1 and HOMO→LUMO+1 configured the main absorption of **NQ-H** with the oscillator strength (f) 0.246, 0.137, and 0.259 respectively. In contrast, the electron transition of

HOMO→LUMO was forbidden with the f being 0.013. The main absorption of **NQ-H** can be calculated based on the energy difference ($\Delta E_{HOMO-1\rightarrow LUMO} = 2.05$ eV, $\Delta E_{HOMO\rightarrow LUMO+1} = 2.54$ eV, and $\Delta E_{HOMO\rightarrow LUMO+2} = 2.09$ eV) as 606, 488, and 592nm. The transition of HOMO–1→LUMO and HOMO→LUMO+2, corresponding to 592 and 606 nm, was in agreement with the experimental value (550-700nm). Due to the weak oscillator strength (0.013), the HOMO→LUMO transition contributes very little to the absorption of **NQ-H**. Although the 472nm absorption decreased upon OH^- addition (Figure 1), there still exist a strong absorption around 472 nm, which corresponds to the calculated HOMO→LUMO+1 transition (488 nm). In summary, it is of the difference in transition energies between **NQ** and **NQ-H**, leading to the significant different absorption character (red shift absorption 610 nm in **NQ-H**). For **NQ**, the electron density distributed over quinoline unit and naphthalimide ring in HOMO. In LUMO, the electron density spread toward to naphthalimide ring mainly. A significant electron distribution at bridging –NH– was found in both HOMO and LUMO. For **NQ-H**, the electron density increased significantly due to the proton departure from the bridging –NH–. In HOMO-1 and HOMO of **NQ-H**, the electron density focused on the bridging –NH– and partly on naphthalimide ring. While, in LUMO of **NQ-H**, the electron density distributed over equally in quinoline and nahthalimide rings. By contrast, the electron moved toward quinolone ring. With the energy level elevated to LUMO+1 and LUMO+2, the electron distribution moved toward quinoline ring furtherly. The character of electron transfer in **NQ-H** is more obvious than that in **NQ**. As shown in Figure 4, the electron is more evenly distributed in **NQ**. However, even distribution was not appeared in **NQ-H**. With the proton departure from –NH–, the energy gap of lowest TDDFT excitation is lowered from 2.50 eV ($\Delta E_{HOMO\rightarrow LUMO}$, **NQ**) to 2.05 eV ($\Delta E_{HOMO\text{-}1\rightarrow LUMO}$, **NQ-H**) and 2.09 eV ($\Delta E_{HOMO\rightarrow LUMO+2}$, **NQ-H**), and therefore results the longest wavelength absorption 610 nm appeared in **NQ-H**. This accounts for the solution color turned to blue upon the addition of OH^-. The higher electron density located on bridge unit enhanced the charger transfer process from the naphthalimide ring to quinoline ring.

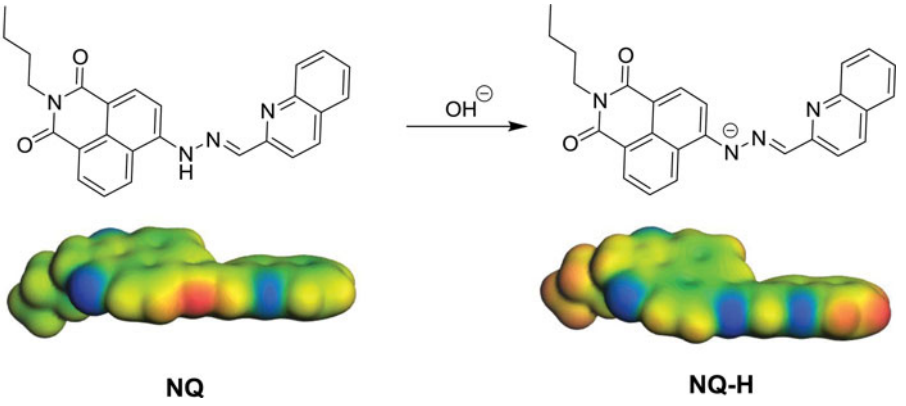

Figure 3. Illustrations of the total electrostatic potential mapped onto the isosurface of the molecular orbital for **NQ** and **NQ-H**. Note: the more negative the values of the potential, the more blue the color.

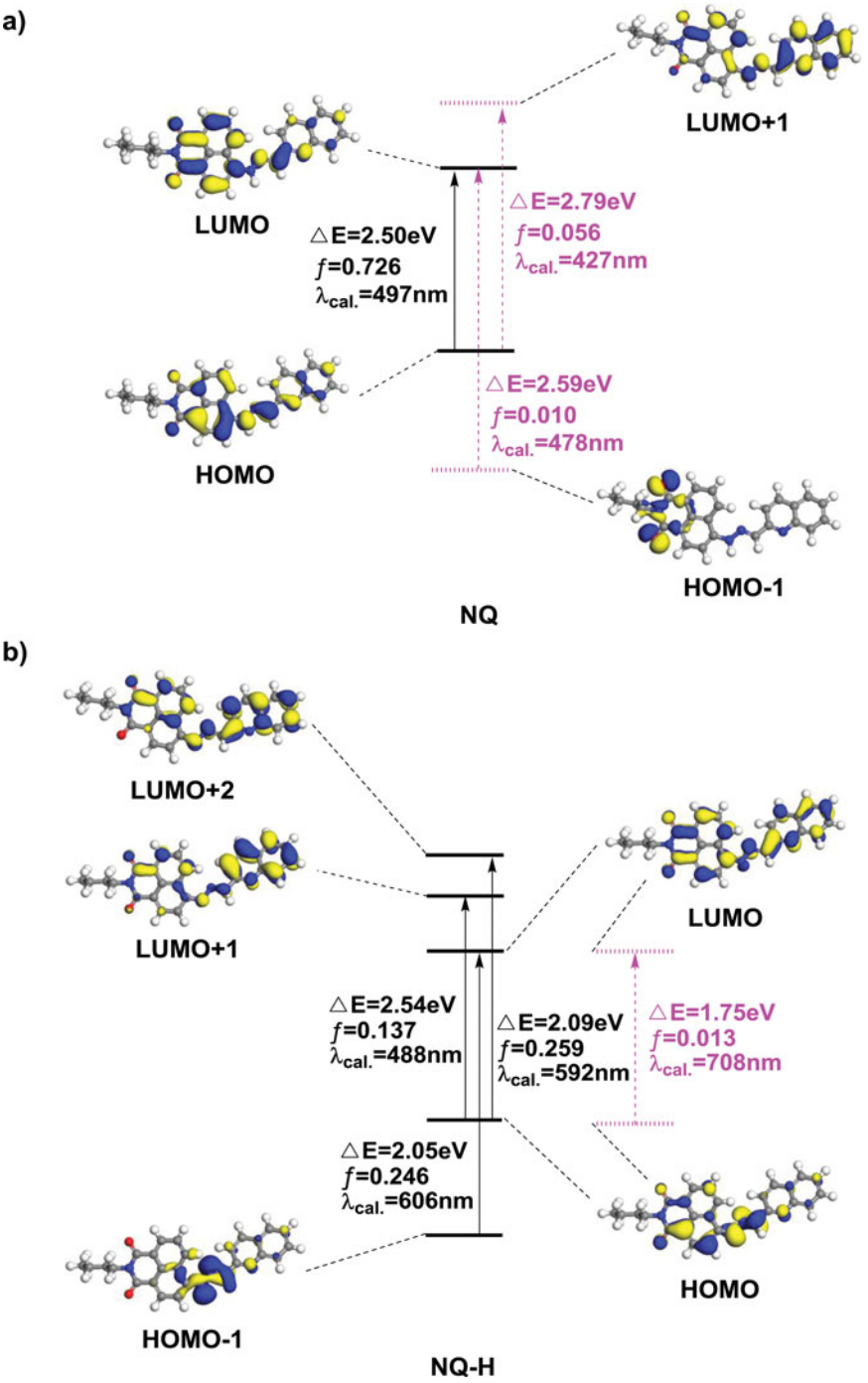

Figure 4. Electron density distributions and energies of the frontier orbitals of **NQ** (a) and **NQ-H** (b).

Conclusions

In summary, a quinline attached to naphthalimide with –NHN– as the bridge unit was synthesized and fully characterized with the NMR and mass technology. Easy deprotonation from bridge unit by base (OH^-) was investigated in detail. Upon the addition of OH^- addition, the intense absorption peak 472nm decreased gradually and new longest absorption maximum centered at 610 nm appeared with obvious isobestic point. At the same time, the solution color turned from yellowish to blue, which is detectable with naked eye. Deprotonation of –NHN– leads to a significant increase of electron density location in N atom. The calculated absorptions for **NQ** and **NQ-H** are also in agreement with the experimental values, supported the experimental results in theory. Enhanced intramolecular charge transfer character, together with the lowered energy gap in electron transition in **NQ-H**, red-shifts the longest absorption maximum.

Acknowledgments

This work was supported by the National Natural Science Foundation of China (grant no. 21272060), University Student Renovation Project (grant no. 201410476085), and Program for Innovative Research Team in Science and Technology in University of Henan Province (15IRTSTHN 003). This study was supported by Basic Science Research Program through the National Research Foundation of Korea (NRF) funded by the Ministry of Science, ICT and Future Planning (Grant no. 2014006660).

References

[1] Loudet, A., & Burgess, K. (2007). *Chem. Rev.*, *107*, 4891.
[2] Li, X., Ma, Y., Wang, B., & Li, G. (2008). *Org. Lett.*, *10*, 3639.
[3] Li, X., Kim, S.-H., & Son, Y. -A. (2009). *Dyes Pigments*, *82*, 293.
[4] Frath, D., Massue, J., Ulrich, G., & Zisessel R. (2014). *Angew. Chem. Int. Ed.*, *53*, 2290.
[5] Li, X., Xu, Y., Wang, B., & Son, Y. -A. (2012). *Tetrahedron Lett.*, *53*, 1098.
[6] Li, X., & Son, Y. -A. (2014). *Dyes Pigments*, *107*, 182.
[7] Ashokkumar, P., Weiβhoff, H., Kraus, W., & Rurack, K. (2014). *Angew. Chem. Int. Ed.*, *53*, 2225.
[8] Li, X., Li, Y., Guo, Z., Kim, H., & Son, Y. -A. (2014). *Fiber. Polym.*, *15*, 914.
[9] Li, X., Chen, X., Zhang, Y., & Son, Y. -A. (2014). *Mol. Cryst. Liq. Cryst.*, *599*, 8.
[10] Li, X., Zhang, Y., Zhao, N., & Son, Y. -A. (2014). *Mol. Cryst. Liq. Cryst.*, *600*, 163.
[11] Wu, Y., Xie, Y., Zhang, Q., Tian, H., Zhu, W., & Li, A. D. Q. (2014). *Angew. Chem. Int. Ed.*, *53*, 2090.
[12] Li, X., Jiang, W., & Son, Y. -A. (2014). *Mol. Cryst. Liq. Cryst.*, *602*, 1.
[13] Li, H., Li, X., Wu, Y., Ågren, H., & Qu, D. -H. (2014). *J. Org. Chem.*, *79*, 6996.
[14] Li, H., Li, X., Ågren, H., & Qu, D. -H. (2014). *Org. Lett.*, *16*, 4940.
[15] Chen, S., Guo, Z., Zhu, S., Shi, W. -E., & Zhu, W. (2013). *ACS Appl. Mater. Interfaces.*, *5*, 5623.
[16] Yao, L., Zhang, S., Wang, R., Li, W., Shen, F., Yang, B., & Ma, Y. (2014). *Angew. Chem. Int. Ed.*, *53*, 2119.
[17] Xiao, P., Dumur, F., Graff, B., Gigmes, D., Fouassier, J. P., & Lalevée, J. (2014). *Macromolecules*, *47*, 601.
[18] Liu, X. -L., Du, X. -J., Dai, C. -G., & Song, Q. -H. (2014). *J. Org. Chem.*, *79*, 9481.
[19] Manjare, S. T., Kim, Y., & Churchill, D. G. (2014). *Acc. Chem. Res.*, *47*, 2985.
[20] Pogozhev, D. V., Bezdek, M. J., Schauer, P. A., & Berlinguette, C. P. (2013). *Inorg. Chem.*, *52*, 3001.
[21] Wu, W., Gue, H., Wu, W., Ji, S., & Zhao, J. (2011). *Inorg. Chem.*, *50*, 11446.

[22] Delley, B. (1990). *J. Chem. Phys.*, *92*, 508.
[23] Delley, B. (2000). *J. Chem. Phys.*, *113*, 7756.
[24] Wang, J., Xu, Z., Zhao, Y., Qiao, W., & Li, Z. (2007). *Dyes Pigments*, *74*, 103.
[25] Gan, J., Tian, H., Wang, Z. H., Chen, K. C., Hill, J., Lane, P. A., Rahn, M. D., Fox, A. M., & Bradley, D. D. C. (2002). *J. Organomet. Chem.*, *645*, 168.
[26] Ivanov, I. P., Dimitrova, M. B., Tasheva, D. N., Cheshmedzhieva, D. V., Lozanov, V. S., & Ilieva, S. V. (2013). *Tetrahedron*, *69*, 712.
[27] Li, X., Zhu, K., Jiang, W., Li, Y., Kim, H., & Son, Y. (2012). *Phys. Status. Solidi. C*, *9*, 2456.
[28] Yang, H., Song, H., Zhu, Y., & Yang, S. (2012). *Tetrahedron Lett.*, *53*, 2026.
[29] Delley, B. (1990). *J. Chem. Phys.*, *92*, 508.
[30] Delley, B. (2000). *J. Chem. Phys.*, *113*, 7756.